Journal of the European Ceramic Society 44 (2024) 3909–3915

Contents lists available at ScienceDirect

Journal of the European Ceramic Society

journal homepage: www.elsevier.com/locate/jeurceramsoc

Spinel-trirutile microwave dielectric ceramics with high Q and excellent temperature stability based on MgO-Al_2O_3-Ta_2O_5 ternary systems

Jian Li [a], Xiaohan Zhang [b], Jia Liu [c], Qingxuan Zhou [a], Haitao Wu [b,*], Yuanyuan Zhou [a], Yang Wang [a], Wei Sun [a], Yanxiang Jiang [a], Yongning Han [a], Zhuoqun Han [a], Zhicheng Zhao [a], Futian Liu [a,*], Walther Glaubitt [c,d], Yongcui Zhang [c], Yingying Wang [c], Ling Li [c,*]

[a] School of Materials Science and Engineering, University of Jinan, Jinan 250022, China
[b] School of Environmental and Material Engineering, Yantai University, Yantai 264005, China
[c] Shandong Industrial Ceramic Research and Design Institute Co., Ltd, Zibo 255000, China
[d] Fraunhofer Institute for Silicate Research ISC, Neunerplatz 2, 97082 Würzburg, Germany

ARTICLE INFO

Keywords:
$MgAl_2O_4$ ceramic
MgO-Al_2O_3-Ta_2O_5
Near-zero τ_f
Ultra-high quality factor

ABSTRACT

(1-x)$MgAl_2O_4$-$x$$MgTa_2O_6$ composite ceramics based on the MgO-Al_2O_3-Ta_2O_5 pseudoternary phase diagram were prepared by the solid-state reaction. $MgAl_2O_4$ and $MgTa_2O_6$ could coexist due to their different crystal structures. $MgAl_2O_4$ inhibited the rapid growth of $MgTa_2O_6$ grains, and dense microstructures (ρ > 95%) with a uniform grain size distribution was obtained, with an optimal densification temperature of 1550 - 1575 °C. The temperature coefficient of resonant frequency (τ_f) and quality factor ($Q\times f$) were optimized by introducing $MgTa_2O_6$ phases with low dielectric loss and positive τ_f. In addition, the partial solid solutions of Al^{3+} into Ta^{5+} sites resulted in loosening bonds within [Al/TaO_6] octahedra and abnormally large polarizabilities, which was confirmed by the decrease in $V_{Ta\text{-}O}$ and the redshift of $A_{1\ g}$(Ta-O) mode. Consequently, the relative permittivity (ε_r) and τ_f values o$_f$ $MgAl_2O_4$-$MgTa_2O_6$ composite ceramics were further enhanced, exceeding the predicted ones. The 0.6$MgAl_2O_4$-0.4$MgTa_2O_6$ composition sintered at 1550 °C achieved excellent performance, with a near-zero τ_f value of 3.3 ± 1.7 ppm/°C, a low ε_r of 16.4 ± 0.3 and an ultra-high $Q\times f$ of 179,000 ± 6700 GHz @ 8.94 ± 0.04 GHz. These findings hold promising applications in the field of 5 G/6 G high-frequency communication.

1. Introduction

With the tremendous demand for Integrated Circuits and millimeter-wave communication, microwave dielectric ceramics (MDCs) have been extensively developed for use in related microelectronic components [1–3]. To minimize inductive crosstalk and signal delay at high frequencies ($T_{PD} = \frac{\sqrt{\varepsilon_r}}{c}$), a low relative permittivity ($\varepsilon_r \leq 15$) is essential for MDCs [4–7]. In addition, MDCs require a high-quality factor (Q > 10, 000 at operating frequency f_0) and a near-zero temperature coefficient of resonant frequency ($\tau_f \sim 0$) for precise frequency selectivity and temperature stability. Developing such material is complicated since the optimization of individual properties leads in opposite directions. Although lattice distortion by doping could optimize τ_f, this inevitably induces a low $Q\times f$ [8]. One effective approach involves combining two phases with opposite τ_f values to control them towards near-zero and sustain high $Q\times f$ values [9].

Spinel ceramics with the general formula AB_2O_4, specifically M_2TiO_4, M_2SiO_4 and MAl_2O_4 (where M = Zn, Mg) are promising materials for millimeter-wave devices due to their high $Q\times f$ and low ε_r ($Q\times f$ > 100,000 GHz, ε_r = 7.5). However, their negative τ_f (−70 ppm/°C) limits practical applications [10,11]. Previous studies have revealed the relationship between structural evolution and the improved microwave dielectric properties of $MgAl_2O_4$ ceramics. Chen et al. [12] highlighted the potential for achieving ultra-high intrinsic $Q\times f$ values of 394, 000 GHz of $MgAl_2O_4$ by suppressing non-intrinsic defects. Takahashi et al. [13–16] improved the cation distribution and $Q\times f$ values of spinel solid solutions. Several other compounds, including (1-x)ZnAl_2O_4-$x$$Mg_2TiO_4$, $MgAl_{2-x}(Zn_{0.5}Ti_{0.5})_xO_4$, (1-$x$)$MgAl_2O_4$-$x$$Mg_2TiO_4$, Mg$Al_2O_4$-$Mg_2GeO_4$, have also achieved satisfactory $Q\times f$ values up to about 180,000 GHz [17–20]. Because these modifications are ineffective in adjusting τ_f values, compensating phases such as TiO_2 and Sr/$CaTiO_3$ were added, which effectively shift the negative τ_f of $MgAl_2O_4$ to near

* Corresponding authors.
E-mail addresses: wuhaitao@ytu.edu.cn (H. Wu), mse_liuft@ujn.edu.cn (F. Liu), kaiye_1980@126.com (L. Li).

https://doi.org/10.1016/j.jeurceramsoc.2024.01.017
Received 18 September 2023; Received in revised form 1 January 2024; Accepted 6 January 2024
Available online 9 January 2024

zero. However, $Q\times f$ values of such composites are below 100,000 GHz due to the high polarization loss [21,22]. Hence, exploring novel compensating material with less dielectric loss, positive τ_f and good chemical compatibility is essential to enhance the dielectric properties of $MgAl_2O_4$-based ceramics.

A previous study indicated that within the xMgO-Ta_2O_5 binary system, $MgTa_2O_6$ possesses impressive microwave dielectric properties, with a high $Q\times f$ and a positive τ_f ($Q\times f > 160{,}000$ GHz, $\tau_f > 30$ ppm/°C) [23]. Through the formation of $MgTa_2O_6$-based solid solutions, the $Q\times f$ values could be further improved [24–26]. In addition, the coexistence of $MgTa_2O_6$ with $MgTiO_3$ or $MgZrTa_2O_8$ has been reported, allowing for control of the composites' τ_f values to near zero [27,28]. These findings suggest that $MgTa_2O_6$ is a potential compensating material for $MgAl_2O_4$. Utilizing the thermodynamic equilibrium approach that avoids chemical reactions proves to facilitate performance optimization through composition [29]. Typically, in a binary or ternary phase diagram, two phases connected by a tie line tend to create a new equilibrium system where the chemical potential gradient difference ($\mu A - \mu B = 0$) is zero. In a MgO-Al_2O_3-Ta_2O_5 pseudoternary phase diagram, a tie line is discovered linking $MgTa_2O_6$ to $MgAl_2O_4$. The compositions positioned along the $MgTa_2O_6$-$MgAl_2O_4$ tie line are investigated to potentially obtain novel composite ceramics with ultra-low dielectric loss and excellent frequency stability. The different crystal structures and adapted sintering temperatures of $MgTa_2O_6$ and $MgAl_2O_4$ could mitigate the influence of structural nonuniformity and prevent co-firing problems. Herein, the (1-x)$MgAl_2O_4$-$x$$MgTa_2O_6$ (Samples 1–6 in Fig. S1 refer to $x = 0.3$, 0.4, 0.5, 0.6, 0.7, 0.8) composite ceramics were synthesized by the solid-state reaction route. Phase compositions, microstructures and crystal structures were systematically investigated and correlated with microwave dielectric properties.

2. Experimental procedure

The high-purity powders of light MgO (Sinopharm Chemical Reagent Co., Ltd., Shanghai, China, 98.5%), Ta_2O_5 (Aladdin Reagent Co., Ltd., Shanghai, China, 99.5%) and Al_2O_3 (Sinopharm Chemical Reagent Co., Ltd., Shanghai, China, 99%) were used as raw materials. MgO was calcinated at 900 °C for 2 h to remove adsorbed carbon dioxide and moisture. The pretreated raw materials were weighed according to the $MgAl_2O_4$ and $MgTa_2O_6$ stoichiometry and then charged into nylon jars with ethanol and zirconia balls for planetary ball-milling for 12 h at 200 rpm. After drying at 70 °C for 5 h and sieving, the uniformly mixed powders were calcined at 1400 °C for 4 h and 1250 °C for 6 h to synthesize $MgAl_2O_4$ and $MgTa_2O_6$, respectively. Afterward, the as-prepared $MgAl_2O_4$ and $MgTa_2O_6$ powders were weighed in an appropriate molar ratio according to the chemical formula of (1-x)$MgAl_2O_4$-$x$$MgTa_2O_6$ ($x = 0.3$, 0.4, 0.5, 0.6, 0.7, 0.8). The mixtures were re-milled for another 12 h at the same speed of 200 rpm and then dried at 70 °C. After granulating with 5 wt% polyvinyl alcohol (PVA), the powders were pressed into cylinders (10 mm × 6 mm) under a uniaxial pressure of 200 MPa. Finally, all samples were heat-treated at 600 °C for 2 h to remove organic residues and sintered at 1525 - 1600 °C for 4 h with a 5 °C/min heating rate. SEM test samples were ground and polished using varigrained metallographic abrasive paper (1000 mesh, 1500 mesh and 2000 mesh) with ethanol step by step. Subsequently, the samples were thermally etched at 50 °C below the sintering temperature for 30 - 60 min

X-ray powder diffraction (D8 Advance, Bruker, Karlsruhe, Germany) with Cu Kα radiation ($\lambda = 1.54060$ Å) was operated to check the phase composition. To analyze detailed information for phase fraction and structure parameters, the measured data were fitted by Rietveld refinement using the FullProf program. Scanning electron microscopy (Model SU8010, Hitachi, Japan) with energy-dispersive spectroscopy (EDS) was performed to observe the microstructure and element distribution of polished and thermally etched ceramic surfaces. SEM image analysis software (Nano Measure System) was used to count the linear intercept of more than 100 clear grains and obtain the average grain size. The distribution histogram of grain size was also plotted using Origin software. Raman spectra were recorded by LabRAM HR Evolution spectrometer with a 532 nm excitation laser. Dielectric properties in the microwave region of (1-x)$MgAl_2O_4$-$x$$MgTa_2O_6$ ceramics were obtained using a vector network analyzer (N5234A, Agilent, USA). Among them, the Hakki–Coleman resonator method [30] was employed to obtain ε_r at 10 - 13 GHz, while the resonant cavity method assessed $Q\times f$ values at 7 - 10 GHz [31,32]. The resonant frequency drift determined τ_f values within a temperature range of 25 - 85 °C, and the calculated formula was expressed as:

$$\tau_f = \frac{f_{85°C} - f_{25°C}}{f_{25°C}(85-25)} \times 10^6 (\text{ppm/°C}) \quad (1)$$

3. Results and discussion

Fig. 1 illustrates the XRD patterns of (1-x)$MgAl_2O_4$-$x$$MgTa_2O_6$ ceramics sintered at 1575 °C for 4 h. The diffraction peaks are assigned to the spinel $MgAl_2O_4$ (ICDD No. 21–1152) and the trirutile $MgTa_2O_6$ (ICDD No. 32–0636). The $MgTa_2O_6$ peaks become stronger relative to the $MgAl_2O_4$ peaks as x increases, indicating that the two phases can coexist effectively. In accordance with the MgO-Ta_2O_5 phase diagram, Mg-rich secondary phases are inevitably generated [23], including a minor quantity of $Mg_5Ta_4O_{15}$ and $Mg_4Ta_2O_9$, as observed in the enlarged figure. As shown in Fig. 1(c, d), the Face-Centered Cubic structure with the $Fd\bar{3}m$ symmetry of $MgAl_2O_4$ comprises edge-sharing [AlO_6] and [MgO_4] polyhedra. In contrast, the trirutile structure of $MgTa_2O_6$ belongs to the $P4_2/mnm$ space group. All Mg^{2+} and Ta^{5+} cations are chemically coordinated, forming [Mg/TaO_6] octahedra connected by O1 and O2 through a common top. The distinct crystal structures contribute to a favorable chemical compatibility between $MgAl_2O_4$ and $MgTa_2O_6$. Nevertheless, the comparable six-fold coordination of [Al/TaO_6] octahedra could potentially result in the formation of partial solid solutions and slightly alter dielectric properties.

To further investigate the phase composition and crystal structures of (1-x)$MgAl_2O_4$-$x$$MgTa_2O_6$ composite ceramics, we conducted Rietveld refinements. The fitted XRD patterns in Fig. S2 (Supplementary Information, SI) closely match the measured data points, demonstrating the reliability of the refinement results. As shown in Fig. S3, the unit cell volume of $MgAl_2O_4$ and $MgTa_2O_6$ decreases with the increase in x possibly because partial Ta^{5+} ions (ionic radius = 0.64 Å) are replaced by Al^{3+} ions (ionic radius = 0.535 Å). Notably, the mass fractions given in Table S1 (Supplementary Information, SI) reveal that as x increases, the secondary phase disappears and the actual phase contents of $MgAl_2O_4$ and $MgTa_2O_6$ approach the intended values.

Fig. 2 displays the bulk densities and relative densities of the (1-x)$MgAl_2O_4$–$x$$MgTa_2O_6$ composite ceramics sintered at various temperatures. Given its theoretical density (~ 7.816 g/cm^3) surpassing that of $MgAl_2O_4$ (~ 3.578 g/cm^3), the addition of $MgTa_2O_6$ results in an increase in the bulk densities of the samples. The relative densities of all samples gradually rise with increasing sintering temperature, corresponding to grain growth and fewer pores. The addition of an appropriate amount of $MgTa_2O_6$ improves the sintering behavior of the composite ceramics, achieving a relative density exceeding 95% at temperatures between 1550 °C and 1575 °C. However, due to oversintering and the formation of internal pores at 1600 °C, the relative densities rapidly decline with more $MgTa_2O_6$ percentages, which degrades high-temperature stability and narrows the sintering temperature window.

Fig. 3 depicts the SEM images of the polished and thermally etched surfaces of (1-x)$MgAl_2O_4$–$x$$MgTa_2O_6$ ceramics ($x = 0.4$, 0.8) sintered at 1575 °C for 4 h. All samples exhibit a dense and non-porous microstructure, aligning with the result of relative density. To determine the chemical compositions of the morphologically distinct grains, the EDS analysis was performed. As analyzed in Fig. S4 (Supplementary

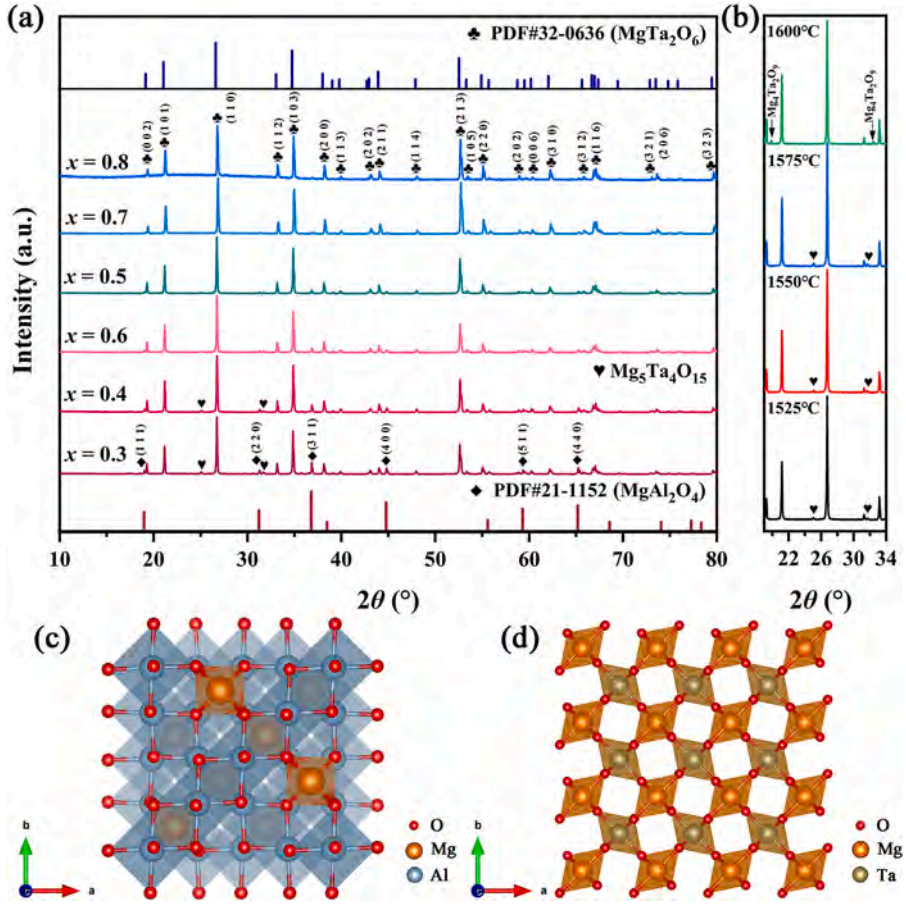

Fig. 1. (a) XRD patterns of (1-x)$MgAl_2O_4$-$x$$MgTa_2O_6$ ceramics sintered at 1575 °C, (b) enlarged XRD patterns of $x = 0.4$ samples sintered at different temperatures, (c) the spinel structure of $MgAl_2O_4$ ceramics, and (d) the rutile structure of $MgTa_2O_6$ ceramics.

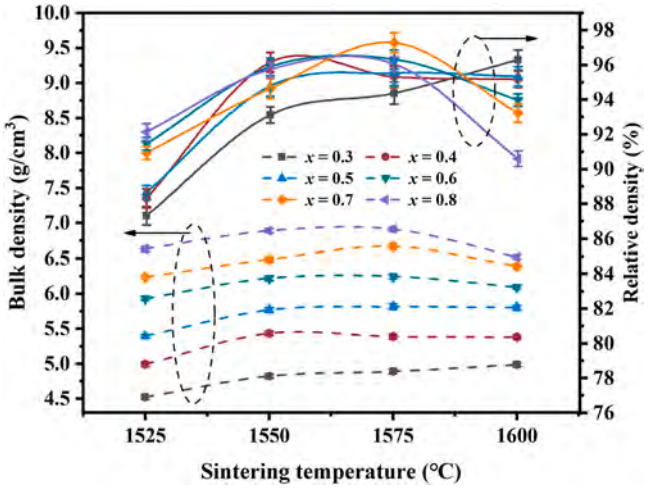

Fig. 2. Bulk densities and relative densities of the (1-x)$MgAl_2O_4$–$x$$MgTa_2O_6$ ceramics ($x = 0.3$ - 0.8) as a function of sintering temperatures.

Information, SI), the equiaxial grain with the Mg to Al molar ratio of 0.54 is identified as $MgAl_2O_4$. The large polygon-like grain with the Mg to Al + Ta) molar ratio of 0.65 is denoted as $MgTa_2O_6$. These findings collectively indicate the coexistence of $MgAl_2O_4$ and $MgTa_2O_6$ phases, with the partial solid solution of Al^{3+} into Ta^{5+} sites. Some Mg-rich phases, such as $Mg_5Ta_4O_{15}$ or $Mg_4Ta_2O_9$, can exist in parallel, possibly due to the partial solid solution and the decomposition of $MgTa_2O_6$ [33]. Moreover, Fig. S5 illustrates how the grain size distribution depends on the phase fraction. Since $MgAl_2O_4$ plays a role in the pinning effect and inhibits the rapid growth of $MgTa_2O_6$ grain, a uniform grain size distribution is obtained. Regrettably, the more $MgTa_2O_6$ is present, the less resistance there is to grain growth, resulting in a bimodal distribution of the grain size in the $x = 0.8$ sample. Rapid grain growth and potential melting of the $MgTa_2O_6$ grains at temperatures above 1600 °C significantly impact the high-temperature stability of the composite ceramics, leading to the formation of internal pores and a decrease in overall performance.

To reveal the inherent connection between lattice vibration and dielectric properties, Raman spectra of (1-x)$MgAl_2O_4$–$x$$MgTa_2O_6$ were studied. Utilizing group theory analysis, the Raman-active vibrational modes of $MgAl_2O_4$ and $MgTa_2O_6$ are deduced from the irreducible representations of $\Gamma = A_{1\,g} + E_g + 3\,T_{2\,g}$ and $\Gamma = 4A_{1\,g} + 2B_{1\,g} + 4B_{2\,g} + 6E_g$, respectively [34,35]. As shown in Fig. 4, a total of 13 Raman active modes of $MgTa_2O_6$ are identified and those of $MgAl_2O_4$ disappear due to the lower intensity and peak overlaps. The modes between 118 and 330.6 cm^{-1} are assigned to Ta-O bending vibrations, including $3E_g$, $B_{1\,g}$, $B_{2\,g}$, and $A_{1\,g}$. The Mg-O coupled vibration generates the E_g and $B_{1\,g}$ modes at 420.2 and 469.1 cm^{-1}, respectively. Additionally, the E_g mode (~ 647.5 cm^{-1}) and the $A_{1\,g}$ mode (~ 706.9 cm^{-1}) result from the Ta-O stretching vibrations, responding sensitively to structural changes in oxygen octahedra [36,37].

Fig. S6 (Supplementary Information, SI) displays the variation in Raman shift and full width at half peak (FWHM) of the $A_{1\,g}$ (Ta-O) mode with the x value. When the volume fractions of the $MgAl_2O_4$ and $MgTa_2O_6$ are close, the $A_{1\,g}$(Ta-O) mode exhibits a blueshift, attributed to the internal compressive stress and contracted [TaO_6] octahedra induced by the differential thermal expansion coefficients and grain

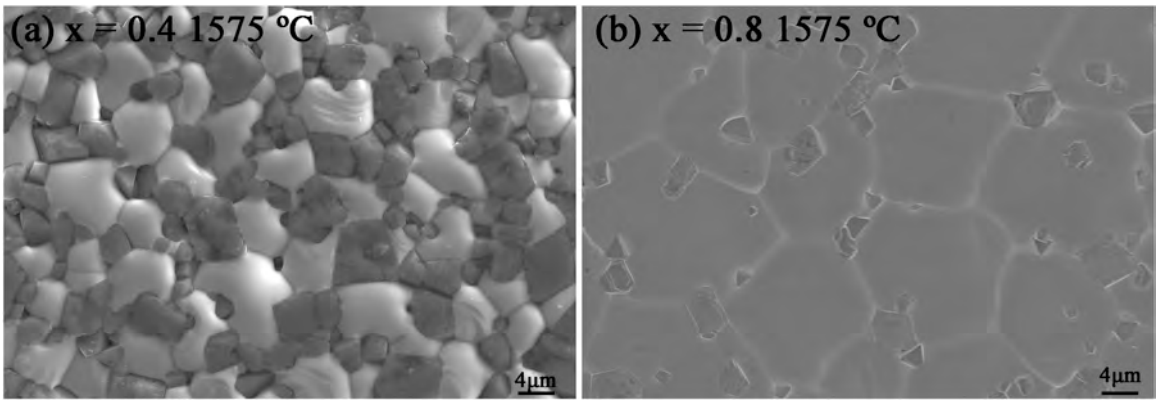

Fig. 3. SEM images of (1-x)$MgAl_2O_4$–$xMgTa_2O_6$ ceramics with $x = 0.4$ and $x = 0.8$ sintered at 1575 °C for 4 h.

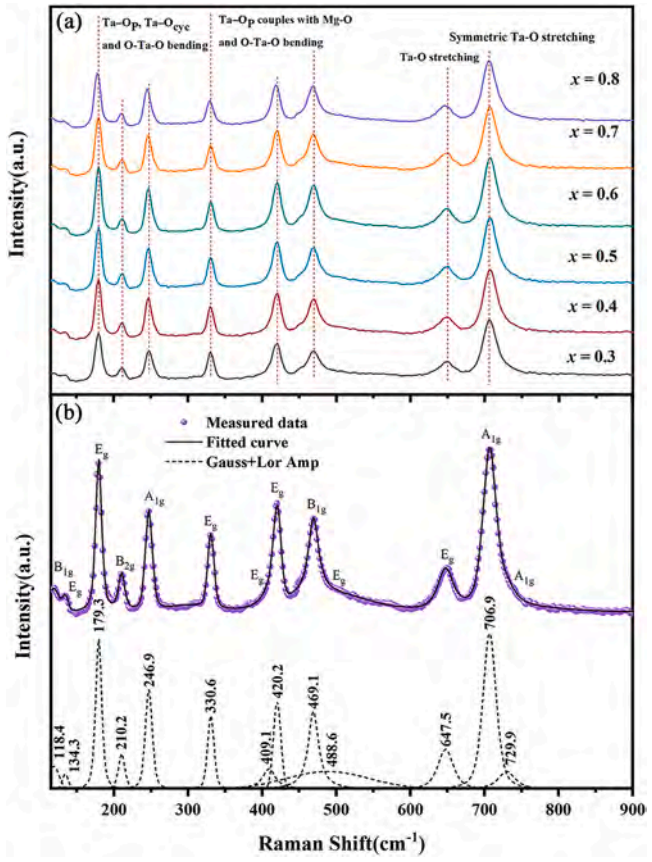

Fig. 4. (a) Raman spectra and (b) peak fitting results of (1-x)$MgAl_2O_4$–$xMgTa_2O_6$ ($0.3 \leq x \leq 0.8$) at room temperature. *Ta-O bonds are simply bridged (Ta-O_P) or doubly bridged, forming a cycle (Ta-O_{cyc}).

growth orientations. This phenomenon may further inhibit the grain growth of $MgTa_2O_6$. As x increases from 0.4 to 0.7, the redshifted A_{1g}(Ta-O) mode implies the weakened Ta-O bonds, corresponding to the increasing bond length detailed in Table S2. The internal stress could affect the lattice spacing and electronic properties, which enhances the anharmonic vibration and dielectric loss. Hence, a strong correlation is determined between the FWHM and the Raman shift of the A_{1g}(Ta-O) mode. In addition, with increasing x, the narrower bandwidth of the A_{1g} mode suggests the improved long-range ordering of the crystal structure and the reduction in the dielectric loss [33].

The variation in ε_r and $Q\times f$ values of the (1-x)$MgAl_2O_4$–$xMgTa_2O_6$ composite ceramics is presented in Fig. 5. The ε_r exhibits a sintering temperature dependence similar to density and increases with a reduction in porosity. The poor high-temperature stability severely degrades the performance of the $x = 0.6$ - 0.8 samples sintered at 1600 °C. As x rises from 0.3 to 0.8, the ε_r of the composite ceramic sintered at optimal temperature increases from 13.6 ± 0.3 to 25.0 ± 0.3. Based on the logarithmic mixing rule (Eq. S1 in Supplementary Information), the theoretical ε_r was calculated and compared with the measured ε_r. The similar variation trend between the measured and calculated values demonstrates that the high permittivity of $MgTa_2O_6$ is the main reason for the enhanced ε_r of the composite ceramic.

The factors influencing $Q\times f$ values, including porosity, phase composition, grain size distribution, and structural defects, are more complicated than those affecting relative permittivity. In Fig. 5(c), the $Q\times f$ values of the (1-x)$MgAl_2O_4$–$xMgTa_2O_6$ ceramics increase and then decline as the sintering temperature rises, and the trend is consistent with that of relative density. The addition of $MgTa_2O_6$ phase with 30 - 60 mol% contributes to improving sintering behavior and enhancing $Q\times f$ values. Nevertheless, excessive $MgTa_2O_6$ leads to a decline in high-temperature stability and performance. Besides porosity, the phase composition significantly affects $Q\times f$ values of composite ceramics, as revealed in Fig. 5(d). Owing to the ultra-low dielectric loss ($Q^{-1} \approx 3.3 \times 10^{-5}$) reported in the literature for $MgTa_2O_6$, the $Q\times f$ value of the (1-x)$MgAl_2O_4$–$xMgTa_2O_6$ ceramics increases with increasing x, fluctuating around the calculated values from Eq. S2 (Supplementary Information, SI). Notably, the rapid growth of $MgTa_2O_6$ grains is hindered, and Al^{3+} cations partially diffuse into Ta^{5+} sites. This results in a uniform grain size distribution and improved long-range cations ordering [33], yielding high $Q\times f$ values of $179{,}000 \pm 6700$ GHz and $182{,}000 \pm 8100$ GHz in the $x = 0.4$ and $x = 0.6$ samples, respectively. The composite ceramics demonstrate superior dielectric properties in the narrow sintering interval of 1550 - 1575 °C, requiring further optimization of sinterability to address the application challenges.

The variation in τ_f values with x is described in Fig. 6. The τ_f value rises from -8.2 ± 2.2 towards 28.5 ± 1.8 ppm/°C with increasing x from 0.3 to 0.8. Based on the mixing rule (Eq. S3 Supplementary Information, SI), the theoretical τ_f of the composite ceramic was calculated, which displays a similar trend to the measured value. The trend with x confirms that the positive τ_f of $MgTa_2O_6$ plays a crucial role in optimizing τ_f values of the (1-x)$MgAl_2O_4$–$xMgTa_2O_6$ composite ceramics. Moreover, the calculated and measured values deviate considerably, yielding a near-zero τ_f around $x = 0.4$ rather than around $x = 0.6$ theoretically. The unexpected difference may result from the structural distortion characterized by the bond distance and bond valence of Al/Ta sites ($V_{Al/Ta\text{-}O}$). According to formulas (2) and (3) [8,36], the bond valence can be calculated:

$$V_i = \sum_j V_{ij} \quad (2)$$

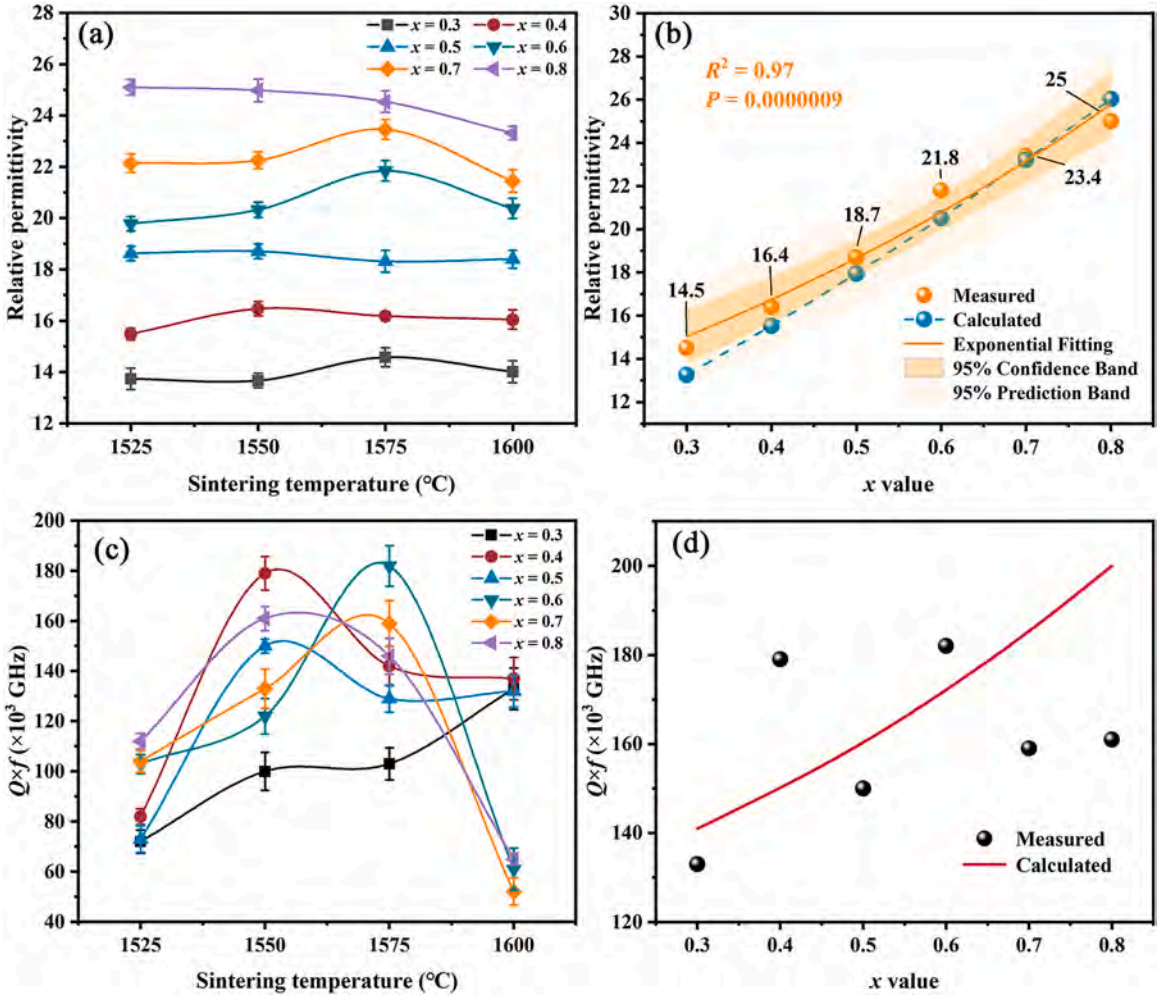

Fig. 5. The relative permittivity and $Q\times f$ values of (1-x)$MgAl_2O_4$–$xMgTa_2O_6$ ceramics as a function of sintering temperatures and x value.

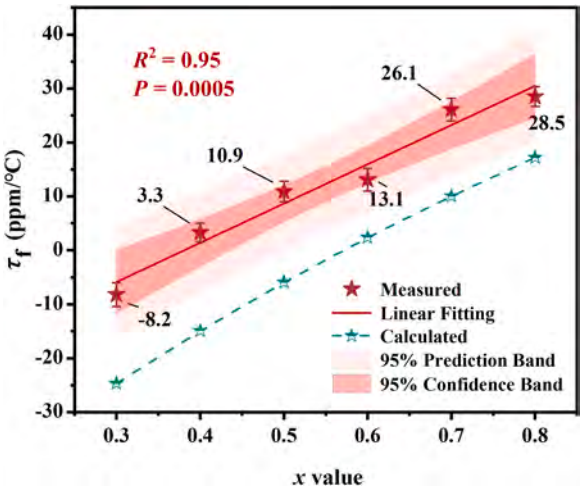

Fig. 6. The measured and calculated τ_f values of (1-x)$MgAl_2O_4$–$xMgTa_2O_6$ ceramics sintered at optimum temperatures versus x value.

$$V_{ij} = \exp\left[\frac{R_{ij} - d_{ij}}{b}\right] \quad (3)$$

where R_{ij} is the bond valence parameter, d_{ij} is the bond length between atoms i and j, and b is a universal constant (0.37 Å). As listed in Table S2 (Supplementary Information, SI), $V_{Al/Ta\text{-}O}$ is lower than the ideal value (2.4 - 2.8 a.u. < 3 a.u. of $V_{Al\text{-}O}$ and 4.1 - 4.5 a.u. < 5 a.u. of $V_{Ta\text{-}O}$), and the $V_{Ta\text{-}O}$ shows a downward trend as x increases. The results indicate that the [Al/TaO_6] octahedra becomes relatively unstable when the partial solid solution occurs, reducing the high-temperature stability of the composite ceramics. In addition, larger bond distances and thermal motions tend to result in abnormally large polarizabilities and decrease the energy required for structural restoration [8], followed by an increase in both ε_r and τ_f. Therefore, the measured values of ε_r and τ_f deviate from the calculated values. The near-zero τ_f of 3.3 ± 1.7 ppm/°C is obtained in the composition with $x = 0.4$ while maintaining a high $Q\times f$ value of 179,000 ± 6700 GHz and the ε_r of 16.4 ± 0.3.

Compared with the other spinel and $MgTa_2O_6$-based ceramics summarized in Table 1 and Fig. 7, the (1-x)$MgAl_2O_4$-$xMgTa_2O_6$ composite ceramics achieve the synergistic optimization for $Q\times f$ and τ_f, offering high-performance dielectric ceramics for 5 G microwave applications. Understanding the phase diagram for the preparation of composite ceramics could initiate a new direction in expanding microwave dielectric ceramic systems with excellent performances.

Table 1
Comparison of sintering temperature and microwave dielectric properties of typical spinel-type and $MgTa_2O_6$-based ceramics.

Compounds (or methods)	S.T. (°C)	ε_r	$Q \times f$ (GHz)	τ_f (ppm/°C)	Ref.
$MgAl_2O_4$	1600/5 h	7.8	85,100	-59.2	[38]
$ZnAl_2O_4$	1600/5 h	8.5	93,300	-60	[15]
$Zn_{0.4}Al_{2.4}O_4$ (molten salt)	1600/5 h	8.2	202,468	-68	[13]
$Mg_{0.4}Al_{2.4}O_4$ (molten salt)	1600/50 h	7.5	232,301	-60	[14]
$MgAl_2O_4$ + 6.4 mol.%LiF	1575/8 h	8.36	99,900	-61.57	[39]
$(Mg_{0.25}Zn_{0.75})Al_2O_4$	1600/5 h	8.4	222,600	-52	[15]
$(Mg_{0.75}Ni_{0.25})Al_2O_4$	1510/3 h	8.21	130,000	-53.5	[40]
$(Mg_{0.8}Co_{0.2})Al_2O_4$	1475/6 h	8.46	49,300	-60	[41]
$(Mg_{0.96}Cu_{0.04})Al_2O_4$	1550/4 h	8.28	72,800	-59	[42]
$Mg_{0.4}Al_{1.2}Ga_{1.2}O_4$	1600/5 h	11.8	191,340	-54	[16]
$ZnAl_{1.9}(Zn_{0.5}Ti_{0.5})_{0.1}O_4$	1400	9.1	115,800	-78	[43]
$MgAl_{1.94}(Mg_{0.5}Ti_{0.5})_{0.06}O_4$	1425/8 h	9.1	98,000	-61.3	[44]
$MgAl_{1.5}(Zn_{0.5}Ti_{0.5})_{0.5}O_4$	1550	9.86	263,900	-92	[18]
$MgAl_{1.8}(Li_{1/3}Ti_{2/3})_{0.2}O_4$	1550	8.78	62,300	-85	[45]
$MgAl_{1.88}(Zn_{0.5}Ti_{0.5})_{0.12}O_4$	1500	8.72	42,036	-5	[18]
$0.79ZnAl_2O_4$-0.21(2MO-TiO_2)M=Co, Mg, Mn	1400–1550	9.6–9.9	23,530–160,800	-66∼− 63	[46]
$0.1MgAl_2O_4$-$0.9Mg_2TiO_4$	1350	12.36	236,600	-61	[19]
Mg_2GeO_4-$MgAl_2O_4$	1600	8.0	150,000	-34	[20]
$0.7Mg_4Nb_2O_9$-$0.15ZnAl_2O_4$-$0.15TiO_2$	1300	13.1	366,000	-60.8	[33]
90 wt%(0.75$ZnAl_2O_4$–0.25TiO_2)− 10 wt%$MgTiO_3$	1450	12.99	69,245	-9.5	[21]
$0.75MgAl_2O_4$-$0.25TiO_2$	1460	11.03	105,400	-12	[22]
$MgTa_{1.92}Sb_{0.08}O_6$	1325	27	109,000	15	[24]
$Mg_{0.94}Mn_{0.06}Ta_2O_6$	1325	28	105,000	19.5	[25]
$Mg_{0.94}Ni_{0.06}Ta_2O_6$	1325	27	173,000	35	[26]
2MgO-Ta_2O_5 + 0.5 wt%B_2O_3	1325	19.9	211,000	8	[23]
$0.7MgTiO_3$-$0.3MgTa_2O_6$	1450	23	81,000	-2	[27]
$0.25MgZrTa_2O_8$-$0.75MgTa_2O_6$	1450	24.88	26,823	-0.5	[28]
$0.7MgAl_2O_4$-$0.3MgTa_2O_6$	1600	14.0 ± 0.4	133,000 ± 8300	-8.2 ± 2.2	This work
$0.6MgAl_2O_4$-$0.4MgTa_2O_6$	1550	16.4 ± 0.3	179,000 ± 6700	3.3 ± 1.7	This work
$0.5MgAl_2O_4$-$0.5MgTa_2O_6$	1550	18.7 ± 0.3	150,000 ± 2700	10.9 ± 1.9	This work

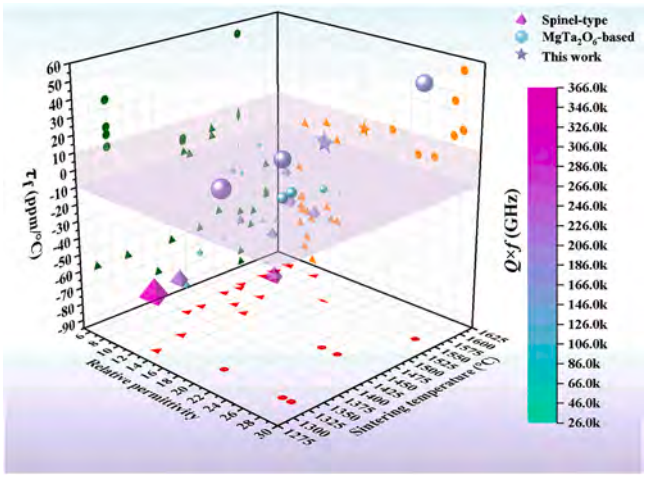

Fig. 7. Summary of relative permittivity, $Q \times f$ values, τ_f values and sintering temperatures for spinel-type and $MgTa_2O_6$-based ceramics.

4. Conclusions

The phase composition, microstructure and microwave dielectric properties of (1-x)$MgAl_2O_4$-$xMgTa_2O_6$ composite ceramics were systematically investigated. The XRD and EDS analysis revealed $MgAl_2O_4$ and $MgTa_2O_6$ as the main crystalline phases along with the partial solution of Al^{3+} into Ta^{5+} sites. The $Q \times f$ and τ_f values of the composite ceramics were optimized due to the low dielectric loss and positive τ_f value of $MgTa_2O_6$. Specifically, excellent dielectric properties were obtained at dense samples with $x = 0.3$ - 0.5 sintered at 1550 - 1575 °C: a series of ε_r of 14.0 ± 0.4 to 18.7 ± 0.3, high $Q \times f$ values of 133,000 ± 8300 to 182,000 ± 8100 GHz and near-zero τ_f of − 8.2 ± 2.2 to 10.9 ± 1.9 ppm/°C. The improved microstructure with porosity-free and uniform grain size distribution correlated the $MgAl_2O_4$ phase to the Zener pinning effect. Moreover, the lower $V_{Ta\text{-}O}$ and the redshift of the $A_{1\,g}$(Ta-O) mode suggested the weakening of the bond strength within [TaO_6] octahedra, resulting in abnormally large polarizabilities and a further increase in both ε_r and τ_f. This work directed a practical processing route to fabricate competitive candidate materials for 5 G/6 G millimeter-wave communications.

CRediT authorship contribution statement

Jian Li: Conceptualization, Methodology, Investigation, Formal analysis, Writing – original draft, Writing – review & editing. **Xiaohan Zhang**: Data curation, Investigation, Validation. **Jia Liu**: Supervision, Writing – review & editing. **Qingxuan Zhou**: Data curation, Investigation. **Haitao Wu**: Methodology, Writing – review & editing, Supervision, Resources, Funding acquisition. **Yuanyuan Zhou**: Methodology, Supervision. **Yang Wang**: Supervision, Writing – review & editing. **Wei Sun**: Supervision, Formal analysis. **Yanxiang Jiang**: Formal analysis. **Yongning Han**: Data curation, Validation. **Zhuoqun Han**: Supervision. **Zhicheng Zhao**: Supervision. **Futian Liu**: Methodology, Visualization, Resources, Supervision, Funding acquisition. **Yongcui Zhang**: Supervision. **Yingying Wang**: Supervision. **Ling Li**: Project administration, Supervision, Investigation, Resources, Funding acquisition. **Walther Glaubitt**: Supervision, Writing – review & editing.

Declaration of Competing Interest

The authors declare that they have no known competing financial interests or personal relationships that could have appeared to influence the work reported in this paper.

Acknowledgements

This research was generously funded by the National Key Research and Development Program of China (Grant No. 2022YFB3706300) and supported by the National Natural Science Foundation of China (Grant No. 52272126).

Appendix A. Supporting information

Supplementary data associated with this article can be found in the online version at doi:10.1016/j.jeurceramsoc.2024.01.017.

References

[1] F. Kamutzki, S. Schneider, J. Barowski, A. Gurlo, D.A.H. Hanaor, Silicate dielectric ceramics for millimetre wave applications, J. Eur. Ceram. Soc. 41 (2021) 3879–3894.

[2] X.Q. Song, F.F. Zeng, J.Q. Yang, C.Z. Yin, J.M. Wu, Y.S. Shi, W.Z. Lu, W. Lei, Crystal structure and microwave dielectric properties of garnet-type $Ca_2YZr_{2-x}Ti_xAl_3O_{12}$ ceramics for dual-band bandpass filters, J. Eur. Ceram. Soc. 42 (2022) 4962–4968.

[3] C.Z. Yin, K. Du, X.Q. Song, Y. Xiong, J.Q. Yang, M.F. Cheng, Y.Y. Cai, W. Luo, H. H. Guo, W.Z. Lu, C.C. Li, W. Lei, A novel low permittivity microwave dielectric ceramic $Sr_2Ga_2SiO_7$ for application in patch antenna, J. Am. Ceram. Soc. 106 (2023) 4284–4293.

[4] X. Zhou, L.T. Liu, J.J. Sun, N.K. Zhang, H.Z. Sun, H.T. Wu, W.H. Tao, Effects of $(Mg_{1/3}Sb_{2/3})^{4+}$ substitution on the structure and microwave dielectric properties of $Ce_2Zr_3(MoO_4)_9$ ceramics, J. Adv. Ceram. 10 (2021) 778–789.

[5] K. Du, C.Z. Yin, Z.Y. Zou, M.F. Cheng, Y.Y. Cai, J.Q. Yang, M. Zhang, W.Z. Lu, S. X. Wang, W. Lei, Correlation between structural characteristics and microwave dielectric properties of walstromite $BaCa_2M_3O_9$ (M = Si, Ge) ceramics, J. Am. Ceram. Soc. 106 (2023) 5822–5831.

[6] J. Bao, Y.P. Zhang, H. Kimura, H.T. Wu, Z.X. Yue, Crystal structure, chemical bond characteristics, infrared reflection spectrum, and microwave dielectric properties of $Nd_2(Zr_{1-x}Ti_x)_3(MoO_4)_9$ ceramics, J. Adv. Ceram. 12 (2023) 82–92.

[7] C. Feng, X. Zhou, B.J. Tao, H.T. Wu, S.F. Huang, Crystal structure and enhanced microwave dielectric properties of the $Ce_2[Zr_{1-x}(Al_{1/2}Ta_{1/2})_x]_3(MoO_4)_9$ ceramics at microwave frequency, J. Adv. Ceram. 11 (2022) 392–402.

[8] Y. Tang, H. Li, J. Li, W.S. Fang, Y. Yang, Z.Y. Zhang, L. Fang, Relationship between Rattling Mg^{2+} ions and anomalous microwave dielectric behavior in $Ca_{3-x}Mg_{1+x}LiV_3O_{12}$ ceramics with garnet structure, J. Eur. Ceram. Soc. 41 (2021) 7697–7702.

[9] Y. Yu, W.J. Guo, Y.C. Zhen, Z.Y. Cen, A. Ji, H. Wu, S.J. Liang, S. Xiong, X.H. Wang, Influence of MnO_2 addition on the dielectric properties of $0.95MgTiO_3$-$0.05CaTiO_3$ ceramics sintered in a reducing atmosphere, J. Eur. Ceram. Soc. 43 (2022) 378–383.

[10] A. Belous, O. Ovchar, D. Durylin, M. Valant, M. Macek-Krzmanc, D. Suvorov, Microwave composite dielectrics based on magnesium titanates, J. Eur. Ceram. Soc. 27 (2007) 2963–2966.

[11] I. Hameed, L. Li, X.Q. Liu, X.M. Chen, Ultra low loss $(Mg_{1-x}Ca_x)_2SiO_4$ dielectric ceramics (x = 0 to 0.15) for millimeter wave applications, J. Am. Ceram. Soc. 105 (2022) 2010–2019.

[12] C.W. Zheng, X.C. Fan, X.M. Chen, Analysis of infrared reflection spectra of $(Mg_{1-x}Zn_x)Al_2O_4$ microwave dielectric ceramics, J. Am. Ceram. Soc. 91 (2008) 490–493.

[13] S. Takahashi, A. Kan, H. Ogawa, Microwave dielectric properties and cation distributions of $Zn_{1-3x}Al_{2+2x}O_4$ ceramics with defect structures, J. Eur. Ceram. Soc. 37 (2017) 3059–3064.

[14] S. Takahashi, H. Ogawa, A. Kan, Electronic states and cation distributions of $MgAl_2O_4$ and $Mg_{0.4}Al_{2.4}O_4$ microwave dielectric ceramics, J. Eur. Ceram. Soc. 38 (2018) 593–598.

[15] S. Takahashi, A. Kan, H. Ogawa, Effects of cation distribution on microwave dielectric properties of $Mg_{1-x}Zn_xAl_2O_4$ ceramics, Mater. Chem. Phys. 200 (2017) 257–263.

[16] A. Kan, H. Okazaki, S. Takahashi, H. Ogawa, Microwave dielectric properties and cation distribution of spinel-structured $Mg_{0.4}Al_{2.4-x}Ga_xO_4$ ceramics with cation defect, Jpn. J. Appl. Phys. 57 (2018) 11UE03.

[17] W. Lei, W.Z. Lu, D. Liu, J.H. Zhu, Phase evolution and microwave dielectric properties of $(1-x)ZnAl_2O_4-xMg_2TiO_4$ ceramics, J. Am. Ceram. Soc. 92 (2009) 105–109.

[18] F. Yang, Y.M. Lai, Y.M. Zeng, Q. Zhang, J. Han, X.L. Zhong, H. Su, Ultra-high quality factor and low dielectric constant of $(Zn_{0.5}Ti_{0.5})^{3+}$ co-substituted $MgAl_2O_4$ ceramic, Ceram. Int. 47 (2021) 22522–22529.

[19] X.Z. Yang, Y.M. Lai, Y.M. Zeng, F. Yang, F.Y. Huang, B.Y. Li, F.S. Wang, C.S. Wu, H. Su, Spinel-type solid solution ceramic $MgAl_2O_4$-Mg_2TiO_4 with excellent microwave dielectric properties, J. Alloy. Compd. 898 (2022) 162905.

[20] S. Deng, X. Qu, X. Wang, Y.Q. Xiao, G.Q. He, K.Y. Liu, Q. Li, Z.L. Dai, X.L. Chen, H. F. Zhou, Solid-phase reaction mechanism and microwave dielectric properties of Mg_2GeO_4-$MgAl_2O_4$ composite ceramics, Ceram. Int. 48 (2022) 31890–31895.

[21] Z.X. He, L. Lu, J.M. Wu, A.N. Chen, S. Chen, L.J. Cheng, S.B. Hua, C.H. Li, C. A. Wang, Y.S. Shi, Microwave dielectric properties of $(0.75ZnAl_2O_4–0.25TiO_2)$–$MgTiO_3$ ceramics prepared using digital light processing technology, J. Am. Ceram. Soc. 105 (2022) 4191–4199.

[22] K.P. Surendran, P.V. Bijumon, P. Mohanan, M.T. Sebastian, $(1-x)MgAl_2O_4-xTiO_2$ dielectrics for microwave and millimeter wave applications, Appl. Phys. A. 81 (2005) 823–826.

[23] M.Z. Dang, H.S. Ren, X.G. Yao, H.Y. Peng, T.Y. Xie, H.X. Lin, L. Luo, Investigation of phase composition and microwave dielectric properties of $MgO-Ta_2O_5$ ceramics with ultrahigh Qf value, J. Am. Ceram. Soc. 101 (2018) 3026–3031.

[24] L. Shi, K. Liu, C. Liu, D.N. Zhang, H.W. Zhang, Investigation of antimony ions doping on crystal structure and enhanced microwave dielectric performance of $MgTa_2O_6$ ceramics, J. Mater. 9 (2023) 701–708.

[25] L. Shi, X.Y. Wang, R. Peng, Y.C. Lu, C. Liu, D.N. Zhang, H.W. Zhang, Effect of Mn^{2+} doping on the lattice and the microwave dielectric properties of $MgTa_2O_6$ ceramics, Ceram. Int. 48 (2022) 20096–20101.

[26] L. Shi, X.Y. Wang, R. Peng, G. Wang, C. Liu, X.L. Shi, D.N. Zhang, H.W. Zhang, Crystallographic characteristics and microwave dielectric properties of Ni-modified $MgTa_2O_6$ ceramics, Ceram. Int. 47 (2021) 22514–22521.

[27] C.L. Huang, K.H. Chiang, Structures and dielectric properties of a new dielectric material system $xMgTiO_3$–$(1-x)MgTa_2O_6$ at microwave frequency, J. Alloy. Compd. 431 (2007) 326–330.

[28] X. Jiang, X.R. Guo, Y. Zhang, S.H. Ding, T.X. Song, A novel $(1-x)MgZrTa_2O_8$–$xMgTa_2O_6$ microwave dielectric composite ceramic with near-zero temperature coefficient, J. Mater. Sci: Mater. Electron 34 (2023) 660.

[29] T. Kolodiazhnyi, $BaMg_{1/3}Nb_{2/3}O_3$–$Mg_4Nb_2O_9$ composite microwave ceramics with high Q-factor and low sintering temperature, J. Eur. Ceram. Soc. 32 (2012) 4305–4309.

[30] B.W. Hakki, P.D. Coleman, A dielectric resonator method of measuring inductive capacities in the millimeter range, IEEE Trans. Microw. Theory Tech. 8 (1960) 402–410.

[31] W.E. Courtney, Analysis and evaluation of a method of measuring the complex permittivity and permeability microwave insulators, IEEE Trans. Microw. Theory Tech. 18 (1970) 476–485.

[32] J. Bao, Y.P. Zhang, H.T. Wu, Y.Y. Zhou, Z.X. Yue, Sintering characteristics, crystal structure and dielectric properties of cobalt-tungsten doped molybdate-based ceramics at microwave frequency, J. Mater. 8 (2022) 949–957.

[33] Y.C. Wu, H.T. Tseng, C.S. Hsi, J. Juuti, H.I. Hsiang, Low dielectric loss ceramics in the $Mg_4Nb_2O_9$-$ZnAl_2O_4$-TiO_2 ternary system, J. Eur. Ceram. Soc. 42 (2022) 448–452.

[34] Y.L. Ma, X.J. Bao, Z.Y. Sui, X.W. Zhao, X. Liu, Quantifying Mg–Al cation distribution in $MgAl_2O_4$-spinel using Raman spectroscopy: An experimental calibration, Solid Earth Sci. 7 (2022) 60–71.

[35] S.F. Jia, Q. Zhou, F.X. Huang, F.F. Li, Y.X. Hu, L.T. Huang, L. Li, Y.N. Li, T. Cui, High-pressure Raman scattering and x-ray diffraction studies of $MgTa_2O_6$, AIP Adv. 10 (2020) 065324.

[36] H.R. Tian, J.J. Zheng, L.T. Liu, H.T. Wu, H. Kimura, Y.Z. Lu, Z.X. Yue, Structure characteristics and microwave dielectric properties of $Pr_2(Zr_{1-x}Ti_x)_3(MoO_4)_9$ solid solution ceramic with a stable temperature coefficient, J. Mater. Sci. Technol. 116 (2022) 121–129.

[37] H.L. Pan, X. Zhou, H.T. Wu, J.L. Du, Z.B. Feng, M. Wübbenhorst, Composition-structure-property relationships in $CeZr_{1.14}Bi_{0.045}A_{0.045}Mo_{4.5}O_{18}$ (A = Nb, Ta and Sb) microwave dielectric ceramics revealed by Raman, far-infrared and terahertz spectra, J. Mater. Res. Technol. 25 (2023) 369–381.

[38] S. Takahashi, A. Kan, H. Ogawa, Microwave dielectric properties and crystal structures of spinel-structured $MgAl_2O_4$ ceramics synthesized by a molten-salt method, J. Eur. Ceram. Soc. 37 (2017) 1001–1006.

[39] T.Y. Qin, C.W. Zhong, Y. Shang, L. Cao, M.X. Wang, B. Tang, S.R. Zhang, Effects of LiF on crystal structure, cation distributions and microwave dielectric properties of $MgAl_2O_4$, J. Alloy. Compd. 886 (2021) 161278.

[40] C.L. Huang, C.Y. Tai, C.Y. Huang, Y.H. Chien, Low-loss microwave dielectrics in the spinel-structured $(Mg_{1-x}Ni_x)Al_2O_4$ solid solutions, J. Am. Ceram. Soc. 93 (2010) 1999–2003.

[41] W.C. Tsai, Y.H. Liou, Y.C. Liou, Microwave dielectric properties of $MgAl_2O_4$–$CoAl_2O_4$ spinel compounds prepared by reaction-sintering process, Mater. Sci. Eng. B 177 (2012) 1133–1137.

[42] B.Y. Li, X.Z. Yang, F. Yang, Y.M. Lai, Q. Zhang, F.S. Wang, C.S. Wu, H.J. Li, H. Su, G. Jiang, Cation distribution driven microstructure and microwave dielectric properties of $Mg_{1-x}Cu_xAl_2O_4$ ceramics, Nanomaterials 12 (2022) 3332.

[43] X.K. Lan, J. Li, Z.Y. Zou, M.Q. Xie, G.F. Fan, W.Z. Lu, W. Lei, Improved sinterability and microwave dielectric properties of $[Zn_{0.5}Ti_{0.5}]^{3+}$-doped $ZnAl_2O_4$ spinel solid solution, J. Am. Ceram. Soc. 102 (2019) 5952–5957.

[44] T.Y. Qin, C.W. Zhong, Y. Qin, B. Tang, S.R. Zhang, The structure evolution and microwave dielectric properties of $MgAl_{2-x}(Mg_{0.5}Ti_{0.5})_xO_4$ solid solutions, Ceram. Int. 46 (2020) 19046–19051.

[45] X. Li, X.Z. Yang, Y.M. Lai, Q. Zhang, B.Y. Li, C. Qi, J. Yin, F.S. Wang, C.S. Wu, H. Su, Improved microwave dielectric properties of $MgAl_2O_4$ spinel ceramics through $(Li_{1/3}Ti_{2/3})^{3+}$ doping, Chin. Phys. B 32 (2022) 057701.

[46] W. Lei, W.Z. Lu, J.H. Zhu, F. Liang, D. Liu, Modification of $ZnAl_2O_4$-based low-permittivity microwave dielectric ceramics by adding 2MO–TiO_2 (M=Co, Mg, and Mn), J. Am. Ceram. Soc. 91 (2008) 1958–1961.